Supporting Information

for

Single Open Sites on Fe^{II} Ions Stabilized by Coupled Metal Ions in CN-Deficient Prussian Blue Analogues for High Catalytic Activity in the Hydrolysis of Organophosphates

Mari Yamane,[†] Hiroyasu Tabe,[†,‡] Masami Kawakami,[§] Hisashi Tanaka,[§] Tohru Kawamoto[§] and Yusuke Yamada*[†,‡]

[†]Department of Applied Chemistry and Bioengineering, Graduate School of Engineering, Osaka City University, 3-3-138 Sugimoto, Sumiyoshi, Osaka 558-8585, Japan

[‡]Research Center of Artificial Photosynthesis (ReCAP), Osaka City University, 3-3-138 Sugimoto, Sumiyoshi, Osaka 558-8585, Japan

[§]Nanomaterials Research Institute, National Institute of Advanced Industrial Science and Technology (AIST), 1-1-1 Higashi, Tsukuba 305-8565, Japan

*E-mail: ymd@a-chem.eng.osaka-cu.ac.jp.

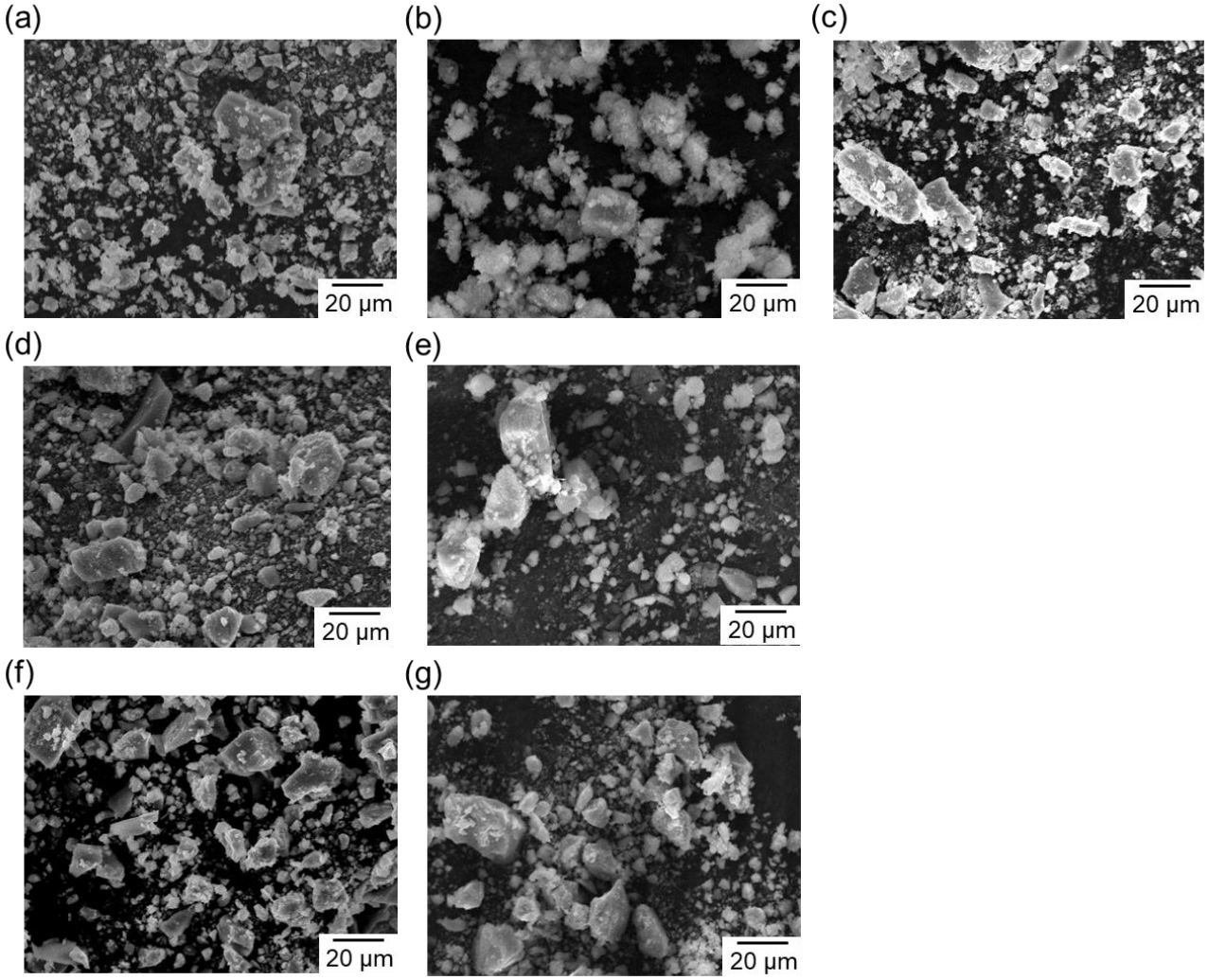

Figure S1. Scanning electron microscope (SEM) images of (a) $[Cu^{II}(H_2O)_{8/3}]_{3/2}[Fe^{II}(CN)_5(NH_3)]$ (**CuFe-NH$_3$**), (b) $[Cu^{II}(H_2O)_2]_{3/2}[Fe^{II}(CN)_6]$ (**CuFe**), (c) $[Cu^{II}(H_2O)_{8/3}]_{3/2}\{[Fe^{II}(CN)_5(H_2O)]_{3/4}[Fe^{II}(CN)_5(NH_3)]_{1/4}\}$ (**CuFe-H$_2$O**), (d) $[Co^{II}(H_2O)_{8/3}]_{3/2}[Fe^{II}(CN)_5(NH_3)]$ (**CoFe-NH$_3$**), (e) $[Co^{II}(H_2O)_2]_{3/2}[Fe^{II}(CN)_6]$ (**CoFe**), (f) $[Ga^{III}(H_2O)][Fe^{II}(CN)_5(NH_3)]$ (**GaFe-NH$_3$**) and (g) $[Ga^{III}(H_2O)_{3/2}]_{4/3}[Fe^{II}(CN)_6]$ (**GaFe**).

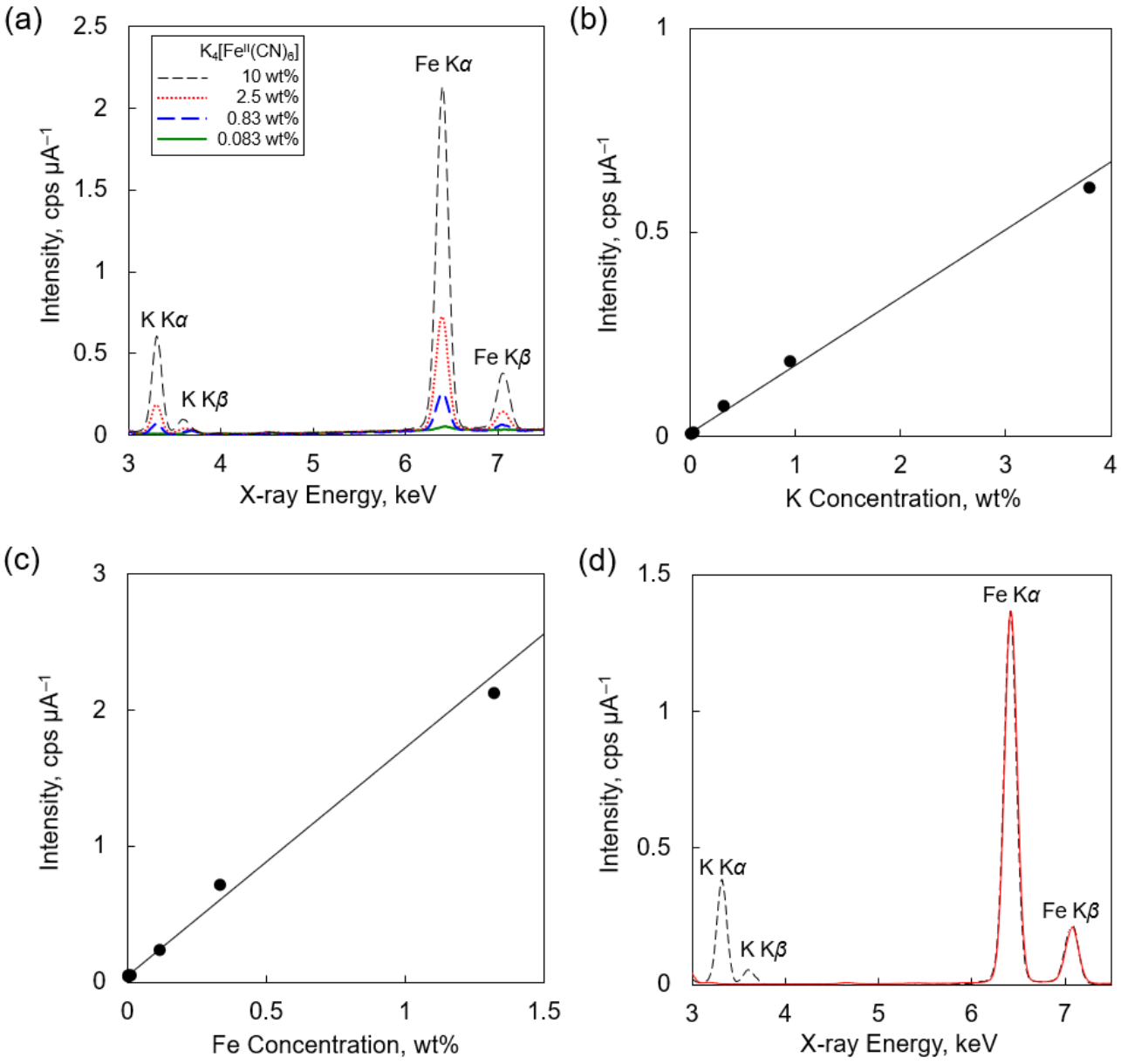

Figure S2. (a) X-ray fluorescence spectra of potassium hexacyanoferrate(II) trihydrate ($K_4[Fe^{II}(CN)_6]\cdot 3H_2O$, 0.083−10 wt%) diluted with silica. (b, c) Peak intensity of (b) K Kα (3.3 keV) or (c) Fe Kα (6.4 keV) as a function of concentrations of K or Fe obtained from (a). (d) X-ray fluorescence spectra of $[Cu^{II}(H_2O)_3]_2[Fe^{II}(CN)_6]$ (**CuFe**, solid line) and $K_4[Fe^{II}(CN)_6]\cdot 3H_2O$ (broken line). No obvious peak of K Kα was observed for **CuFe.**

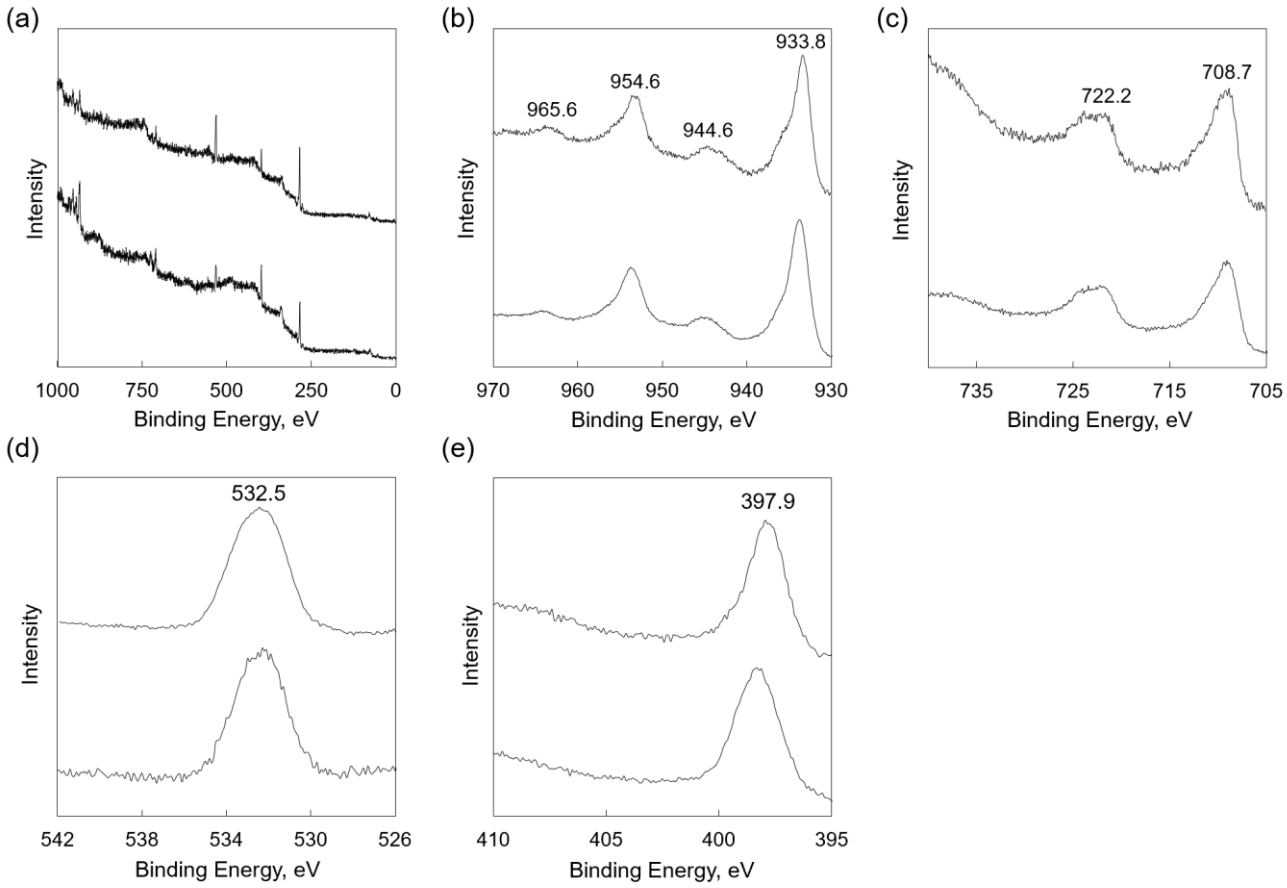

Figure S3. (a) Overall X-Ray photoelectron (XPS) spectra and magnified views in the binding energy regions of (b) Cu 2p, (c) Fe 2p (d) O 1s and (e) N 1s for **CuFe-NH$_3$** (upper lines) and **CuFe** (lower lines).

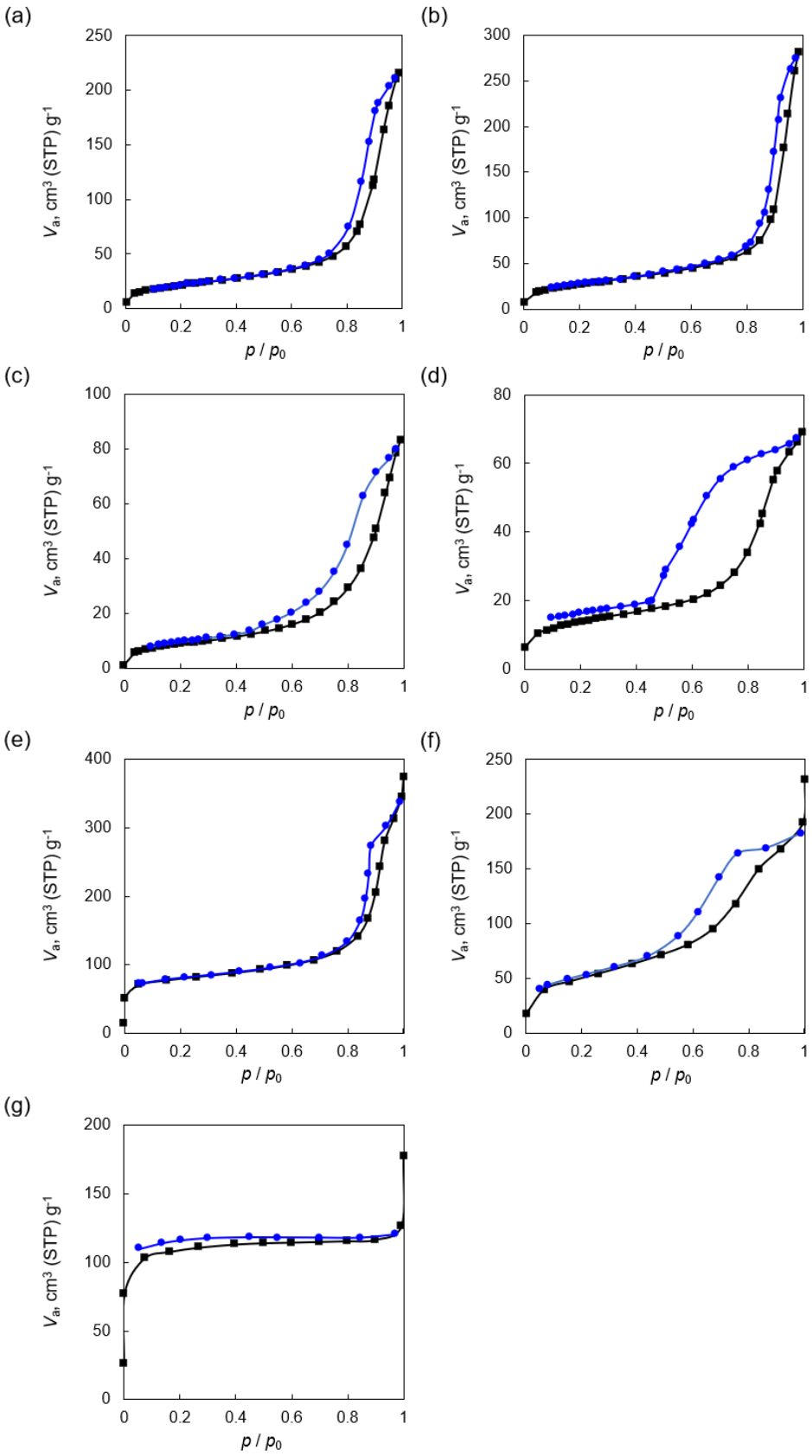

Figure S4. Nitrogen adsorption (■)–desorption (●) isotherms of (a) $[Cu^{II}(H_2O)_{8/3}]_{3/2}[Fe^{II}(CN)_5(NH_3)]$ (**CuFe-NH₃**), (b) $[Cu^{II}(H_2O)_2]_{3/2}[Fe^{II}(CN)_6]$ (**CuFe**), (c) $[Cu^{II}(H_2O)_{8/3}]_{3/2}[Fe^{II}(CN)_5(H_2O)]$ (**CuFe-H₂O**), (d) $[Co^{II}(H_2O)_{8/3}]_{3/2}[Fe^{II}(CN)_5(NH_3)]$ (**CoFe-NH₃**), (e) $[Co^{II}(H_2O)_2]_{3/2}[Fe^{II}(CN)_6]$ (**CoFe**), (f) $[Ga^{III}(H_2O)][Fe^{II}(CN)_5(NH_3)]$ (**GaFe-NH₃**) and (g) $[Ga^{III}(H_2O)_{3/2}]_{4/3}[Fe^{II}(CN)_6]$ (**GaFe**).

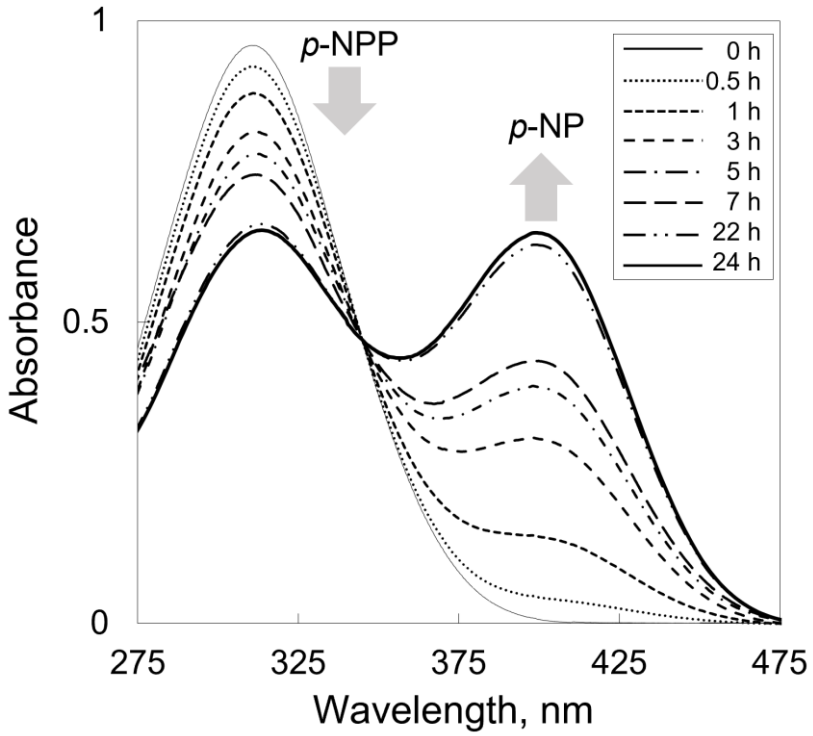

Figure S5. UV-Vis spectral change by hydrolysis of disodium *p*-nitrophenyl phosphate (*p*-NPP, 25 mM) in a HEPES buffer solution (100 mM, 0.75 mL, pH 6.0) containing $[Cu^{II}(H_2O)_{8/3}]_{3/2}[Fe^{II}(CN)_5(NH_3)]$ (**CuFe-NH$_3$**, 0.063 mmol of Fe) at 50 °C. An aliquot (10 μL) of the reaction mixture was periodically sampled and diluted with HEPES buffer solution (100 mM, 2490 μL, pH 8.3). The peaks at 315 and 400 nm are assignable to *p*-NPP and *p*-nitrophenolate ion (*p*-NP), respectively.

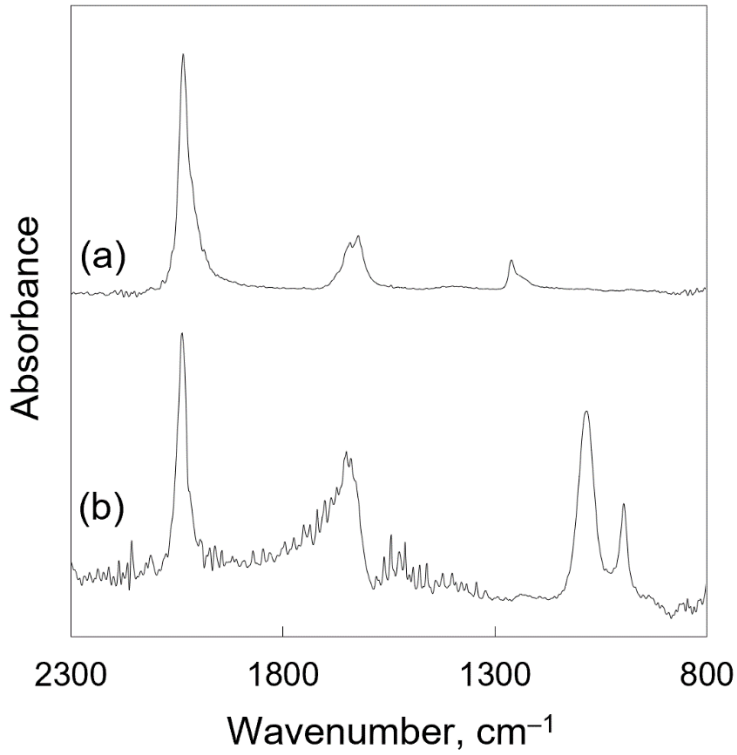

Figure S6. Infrared (IR) spectra of aqueous solutions containing (a) pentacyanoammineferrate ion ($[Fe^{II}(CN)_5(NH_3)]^{3-}$, 100 mM) and (b) $[Fe^{II}(CN)_5(NH_3)]^{3-}$ (100 mM) and hydrogen phosphate (HPO_4^-, 100 mM).

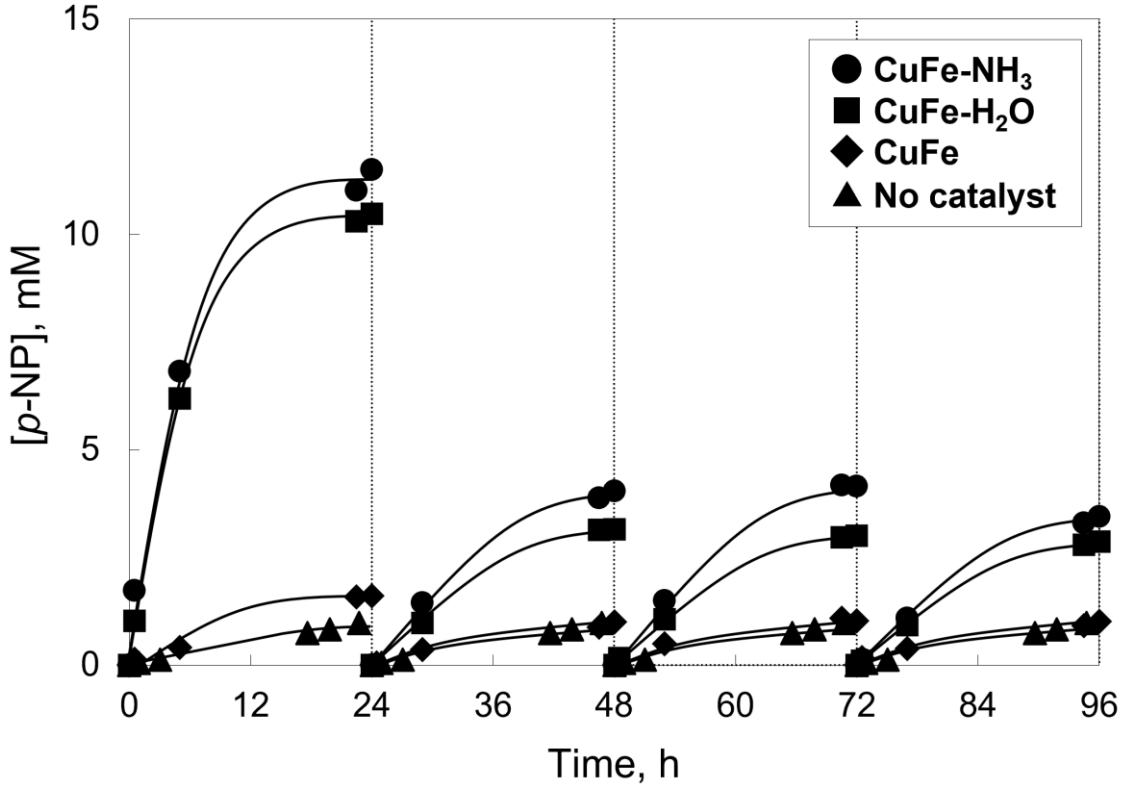

Figure S7. Time profiles of the *p*-nitrophenolate ion (*p*-NP) formation in a HEPES buffer solution (100 mM, 0.75 mL, pH 6.0) containing disodium *p*-nitrophenyl phosphate (*p*-NPP, 25 mM) in the absence and presence of $[Cu^{II}(H_2O)_{8/3}]_{3/2}[Fe^{II}(CN)_5(NH_3)]$ (**CuFe-NH3**), $[Cu^{II}(H_2O)_{8/3}]_{3/2}\{[Fe^{II}(CN)_5(H_2O)]_{3/4}[Fe^{II}(CN)_5(NH_3)]_{1/4}\}$ (**CuFe-H2O**) and $[Cu^{II}(H_2O)_3]_2[Fe^{II}(CN)_6]$ (**CuFe**) (0.063 mmol of Fe) at 50 °C. Catalysts were centrifugally recovered from the reaction solution for a next run.

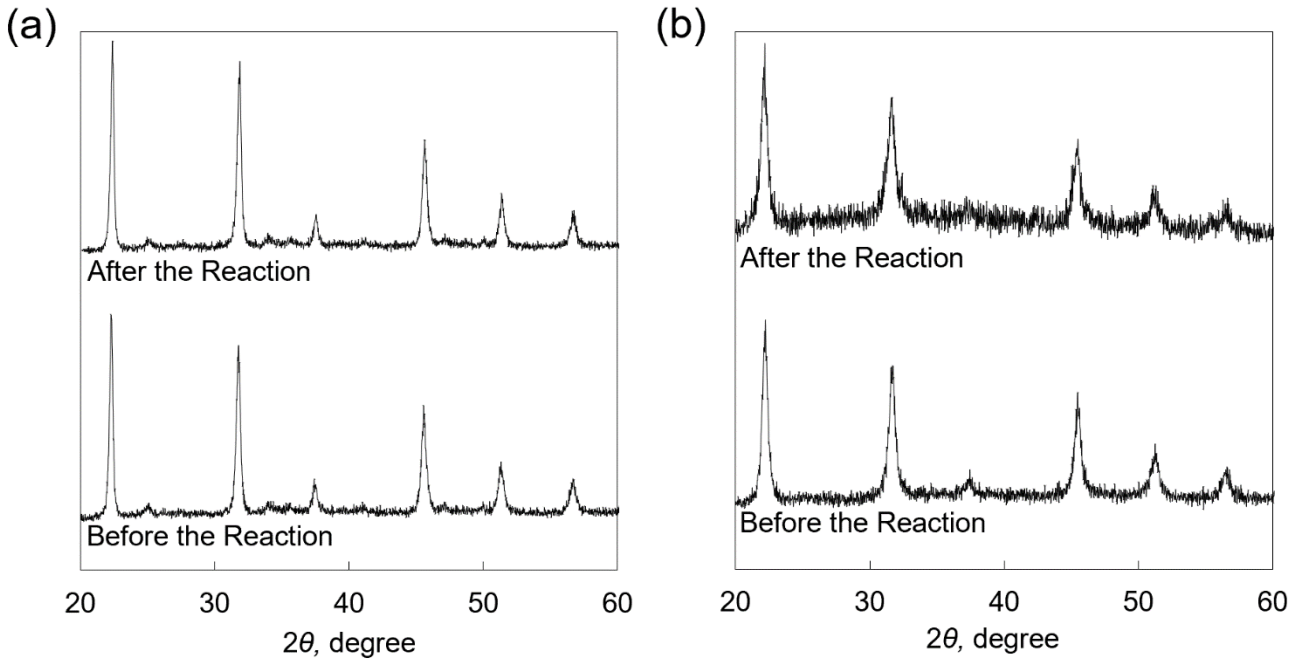

Figure S8. Powder X-ray diffraction patterns of (a) $[Cu^{II}(H_2O)_3]_2[Fe^{II}(CN)_6]$ (**CuFe**) and (b) $[Cu^{II}(H_2O)_{8/3}]_{3/2}[Fe^{II}(CN)_5(NH_3)]$ (**CuFe-NH$_3$**) before and after catalytic hydrolysis of disodium *p*-nitrophenyl phosphate (*p*-NPP, 25 mM) in a HEPES buffer solution (100 mM, 0.75 mL, pH 6.0, 50 °C) for 24 h.

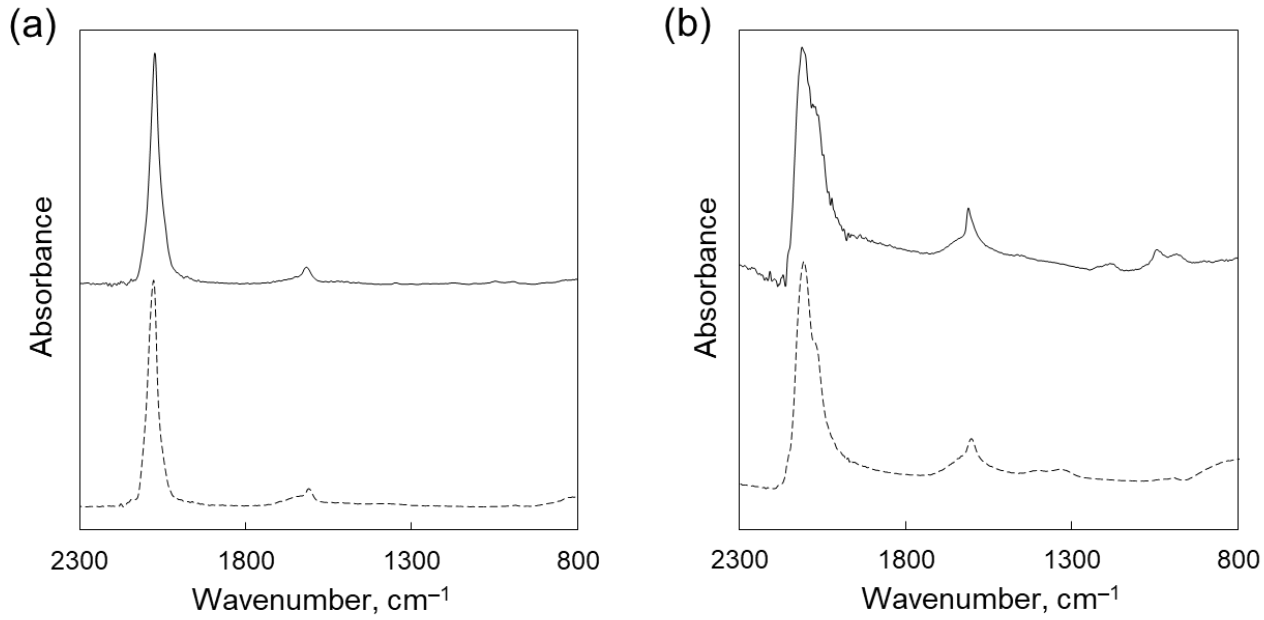

Figure S9. Infrared (IR) spectra of (a) $[Co^{II}(H_2O)_3]_2[Fe^{II}(CN)_6]$ (**CoFe**) and (b) $[Ga^{III}(H_2O)_{3/2}]_{4/3}[Fe^{II}(CN)_6]$ (**GaFe**) before (broken lines) and after (solid lines) catalytic hydrolysis of disodium *p*-nitrophenyl phosphate (*p*-NPP, 25 mM) in a HEPES buffer solution (100 mM, 0.75 mL, pH 6.0, 50 °C) for 24 h.

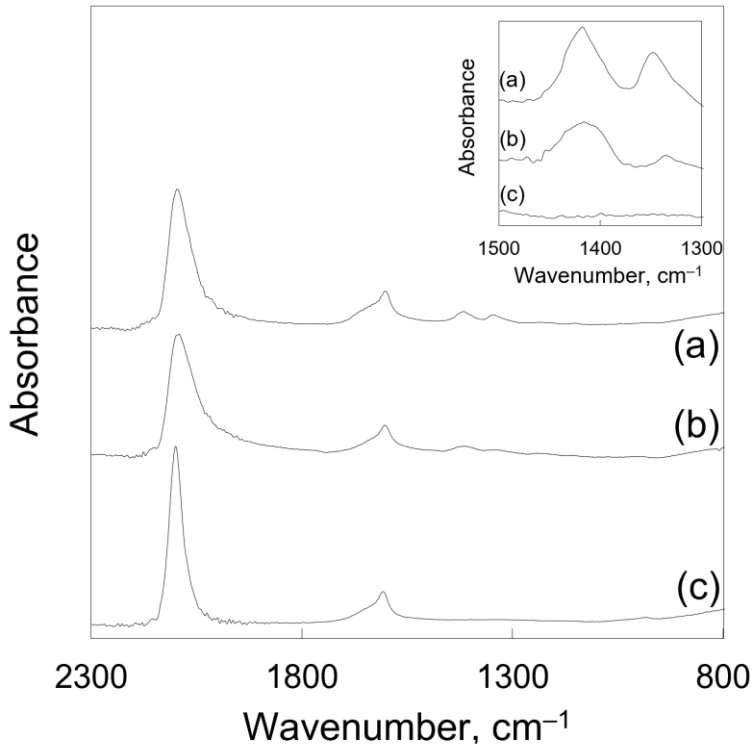

Figure S10. Infrared (IR) spectra of (a) $[Cu^{II}(H_2O)_{8/3}]_{3/2}[Fe^{II}(CN)_5(NH_3)]$ (**CuFe-NH3**), (b) $[Cu^{II}(H_2O)_{8/3}]_{3/2}\{[Fe^{II}(CN)_5(H_2O)]_{3/4}[Fe^{II}(CN)_5(NH_3)]_{1/4}\}$ (**CuFe-H2O**) and (c) $[Cu^{II}(H_2O)_3]_2[Fe^{II}(CN)_6]$ (**CuFe**) obtained by the attenuated total reflection (ATR) technique. Magnified view of the δ_{HNH} region (1300−1500 cm^{-1}) is shown in the inset.

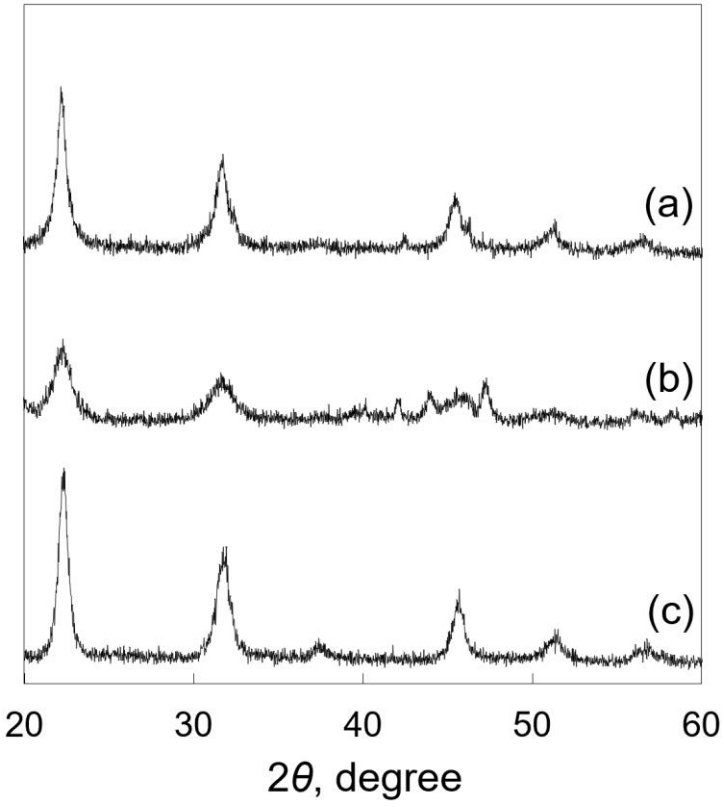

Figure S11. Powder X-ray diffraction (PXRD) patterns of (a) $[Cu^{II}(H_2O)_{8/3}]_{3/2}[Fe^{II}(CN)_5(NH_3)]$ (**CuFe-NH$_3$**), (b) $[Cu^{II}(H_2O)_{8/3}]_{3/2}\{[Fe^{II}(CN)_5(H_2O)]_{3/4}[Fe^{II}(CN)_5(NH_3)]_{1/4}\}$ (**CuFe-H$_2$O**) and (c) $[Cu^{II}(H_2O)_3]_2[Fe^{II}(CN)_6]$ (**CuFe**).

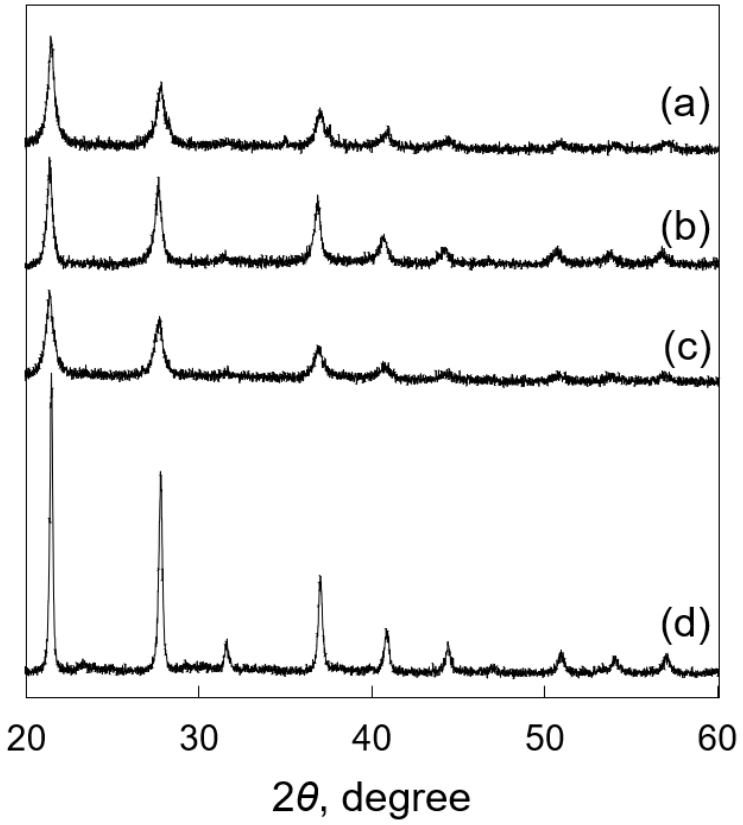

Figure S12. Powder X-ray diffraction (PXRD) patterns of $[Cu^{II}(H_2O)_x]_y\{[Fe^{II}(CN)_5(NH_3)]_n[Fe^{II}(CN)_6]_{1-n}\}$ complexes. [(a) n = 1, (b) n = 0.83, (c) n = 0.5 and (d) n = 0]

Table S1. Concentrations of iron (Fe) and sodium (Na), and their molar ratio (Na/Fe) in the digested solutions of $[Cu^{II}(H_2O)_3]_2[Fe^{II}(CN)_6]$ (**CuFe**, 190 μg L^{-1}), $[Cu^{II}(H_2O)_{8/3}]_{3/2}[Fe^{II}(CN)_5(NH_3)]$ (**CuFe-NH$_3$**, 36 μg L^{-1}) and $[Cu^{II}(H_2O)_{8/3}]_{3/2}[Fe^{II}(CN)_5(H_2O)]$ (**CuFe-H$_2$O**, 71 μg L^{-1}) determined by inductively coupled plasma optical emission spectroscopy (ICP-OES) analyses

PBA	Fe concentration, μg L^{-1}	Na concentration, μg L^{-1}	Molar ratio (Na/Fe)
CuFe	25.12	0.46	0.044
CuFe-NH$_3$	45.83	0.50	0.026
CuFe-H$_2$O	56.88	0.50	0.021

Table S2. Concentrations of phosphorus (P) and their molar ratio of (P/Fe) in the digested solutions of $[Cu^{II}(H_2O)_{8/3}]_{3/2}[Fe^{II}(CN)_5(NH_3)]$ (**CuFe-NH$_3$**, 41.16 mg mL^{-1}) and $[Cu^{II}(H_2O)_3]_2[Fe^{II}(CN)_6]$ (**CuFe**, 42.04 mg L^{-1}) determined by inductively coupled plasma mass spectrometry (ICP-MS) analyses

PBA	Fe concentration, μg L^{-1}	P concentration, μg L^{-1}	Molar ratio (P/Fe)
CuFe-NH$_3$	4.68	0.056	0.12
CuFe	5.33	0.18	0.021